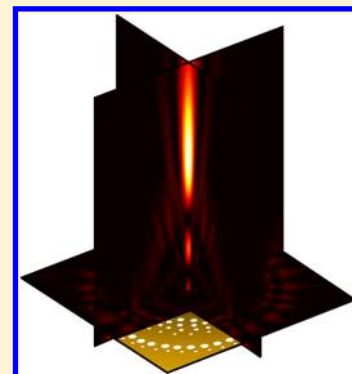


Holey-Metal Lenses: Sieving Single Modes with Proper Phases

Satoshi Ishii, Vladimir M. Shalaev, and Alexander V. Kildishev*

Birk Nanotechnology Center, School of Electrical and Computer Engineering, Purdue University, West Lafayette, Indiana 47907, United States

ABSTRACT: We study a planar, holey-metal lens made as a set of concentric circular arrays (rings) of nanoscale holes milled in a subwavelength-thick metal film. Each nanohole—a finite-length, circular, single-mode waveguide with a radius-dependent mode index—is used as a phase-shifting element. Our experimental results confirm that the focusing properties of our polarization-independent, holey-metal lens milled in a 380-nm-thick gold film and illuminated with 531 nm light fits the analytical model well. The proposed concept could offer an alternative to conventional refraction microlenses and open up a vital path toward on-chip or fiber-end planar photonic devices for biosensing and imaging.



KEYWORDS: Planar lens, diffraction lens, plasmonic lens, phase control

Scaling down optical elements is essential for making compact optical systems. In this regard, planar and thin structures are desirable for fabrication as well as for integration simplicity. Current dielectric-based refraction microlenses typically have a nonuniform thickness of a few tens of micrometers. Gradient-index lenses are planar, but the thicknesses are about an order of magnitude larger than the operational wavelength, and the fabrication process is not straightforward. Classical focusing devices such as Fresnel zone plates are planar and thin, but they do not gradually control the phase at the subwavelength scale. Phase-controlled diffractive microlenses present a hybrid system between a diffraction lens and a refraction lens and have been studied experimentally¹ as well as numerically,^{2,3} but the structures are not planar.

Recently, there has been growing interest in planar, subwavelength-thick metallic lenses for use in the optical wavelength range. Several different designs for metallic lenses have been proposed and experimentally demonstrated, such as superlenses,^{4–6} hyperlenses,^{7–10} surface-plasmon focusing lenses,^{11,12} and superoscillation-based lenses.^{13–15} Some of these metallic lenses create focus spots on a surface,^{11,12} while others focus in the far field.^{16,17} Nanoslit lenses are a type of planar metallic lens consisting of arrays of subwavelength slits milled in a metallic film. Each slit width is varied to change the mode index for single-mode light propagating through the slit, such that light transmitted through different slits experiences different phase delays. In this way, the phase front of the overall transmitted beam can be tailored by appropriately designing the slits. For example, by using a symmetric array of slits with decaying phase shifts relative to the optic axis, it is possible to arrange a concave phase front and focus linearly polarized transmitted light. The very first designs of nanoslit metal lenses were modeled numerically^{18,19} and then demonstrated experimentally.²⁰ All of the early work dealt with plasmonic

mode propagation through the metallic slits. In our recent work, we showed that photonic modes also can be used efficiently to introduce a phase delay.²¹ The use of either a plasmonic mode or a photonic mode enabled us to design polarization-selective nanoslit lenses whose focusing attributes provide either a convex (light-focusing) or concave (light-diverging) lens depending on the incident linear polarization. In addition to static focusing, the focusing properties of nanoslit lenses can be modulated by incorporating liquid crystals inside the slits.²²

Although nanoslit lenses are indeed planar and quite thin, an important drawback of the nanoslit design is its polarization dependence. Moreover, because a nanoslit lens focuses light into a narrow stripe, the design does not allow for high-intensity confinement of light in a wavelength-sized circular spot. For some applications, these drawbacks hinder the use of nanoslit lenses in practical applications. In this Letter, we eliminate these undesirable features of nanoslit lenses by extending the concepts of one-dimensional nanoslit lenses (see Figure 1A) into two dimensions. A natural extension would be simply milling concentric circular slits with different widths in a metallic film (see Figure 1B). However, this approach is limited because linearly polarized light will never focus into a circular spot. By way of an example, for y -polarized light, as schematically shown in Figure 1B, some parts of the circular slits where the incident electric field (E -field) is parallel to the radial direction will perform as slit waveguides under transverse magnetic (TM) excitation, while other parts of the slits where the E -field is normal to the radial direction will perform as slit

Received: October 7, 2012

Revised: December 7, 2012

Published: December 17, 2012

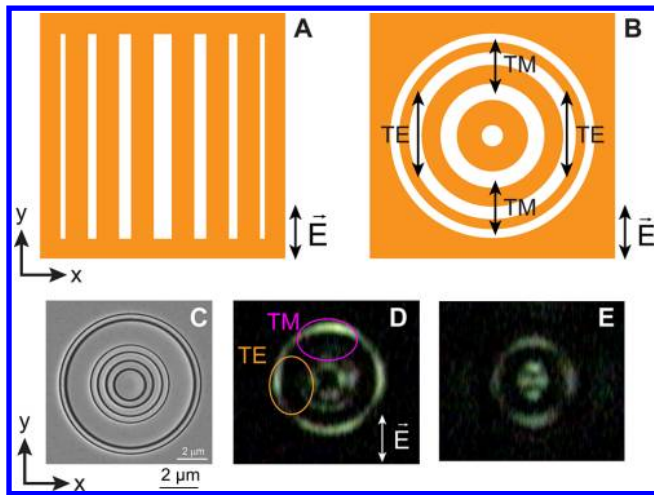


Figure 1. (A) Schematic of a nanoslit lens. (B) Schematic of a device with concentric rings. (C) Scanning electron microscopy (SEM) image of a sample with six concentric rings milled into a 380-nm-thick gold film. (D and E) Experimentally captured charge-coupled device (CCD) images of the sample at the surface ($z = 0 \mu\text{m}$) and at the focus ($z = 10 \mu\text{m}$), respectively. The polarization is parallel to the y -axis. The scales and the coordinates of D and E are identical to the scale and the coordinate system of C.

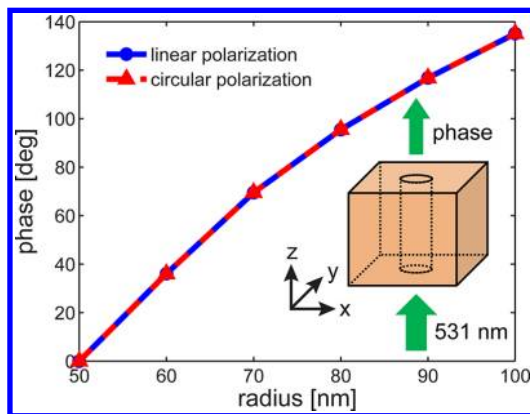


Figure 2. Numerically evaluated relative phase for linearly polarized and circularly polarized 531 nm plane waves transmitted through a variable-radius hole in a 380-nm-thick gold film in the far field.

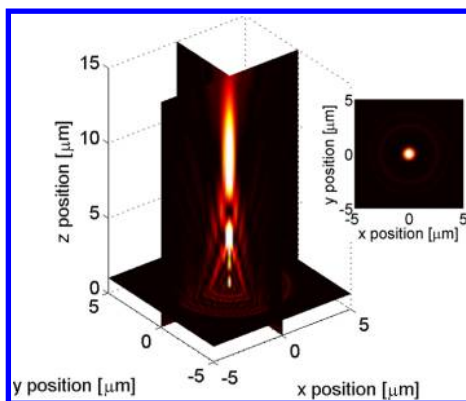


Figure 3. Pseudocolor intensity map of calculated from the analytical model of the sample. The color scale is normalized to the maximum intensity. The inset shows the beam cross section at the focal point ($z = 10 \mu\text{m}$).

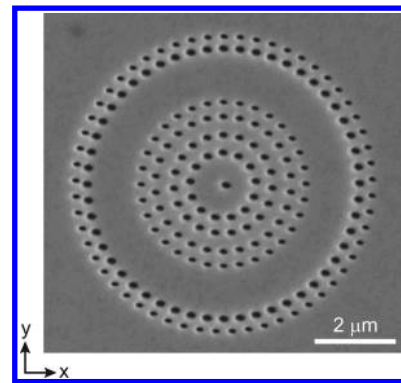


Figure 4. SEM image of the holey metal lens sample before the PMMA spin-coating process.

Table 1. Design Parameters of the Sample Shown in Figure 4

concentric ring no.	1	2	3	4	5	6	7
distance from the origin (μm)	0	0.8	1.2	1.6	2.0	3.3	3.63
hole radius (nm)	83	76	69	62	56	83	56
no. holes	1	13	19	26	32	52	57

waveguides under transverse electric (TE) polarization. This causes undesirable differences in the way TM and TE light interact with the slits because the mode index versus width dependence are opposite for TM-polarization (a plasmonic mode) and TE polarization (a photonic mode).²² Thus the design in Figure 1B does not focus light into a circular spot unless either the slit widths are nonuniform or the slits are noncircular. Therefore, for arbitrarily polarized light, the axial symmetry of the design is lost with this approach, and the performance of the device becomes strongly polarization-dependent.

To demonstrate the focusing properties of the slit-ring lens schematically shown in Figure 1B, we fabricated and recorded the intensity of the 531 nm light transmitted through a sample that has subwavelength-size concentric rings as we will describe later in the paper. The SEM image of the fabricated sample is shown in Figure 1C, and the CCD images at the surface ($z = 0 \mu\text{m}$) and at the focus ($z = 10 \mu\text{m}$) are shown in Figure 1D and E, respectively. Figure 1E clearly indicates that the focal spot does not have a circular profile due to the nonuniform transmission through the rings (Figure 1D). Similar transmission properties were confirmed by numerical simulations.^{23,24} Note that this design can focus radially polarized light, although radial polarization is not a conventional output polarization state from typical light sources.

To focus arbitrarily polarized light and to avoid design complexities, we discretized each circular slit into a circular array of equidistant, identical holes so that our entire design is now arranged as a set of concentric arrays (rings) of holes. The phase front of the transmitted light is controlled by adjusting the radii of the holes in each ring. There are a few previous studies that have investigated similar designs to ours, although none of them have explored phase control by means of changing the hole radii.^{24–26} Because our design supports axial symmetry both globally (in the rings of holes) and locally (for each circular hole), the device can focus normally incident, linearly polarized light with any polarization angle. We also note that our design may appear topologically similar to photon sieves,^{27–31} which have been used to improve the focusing

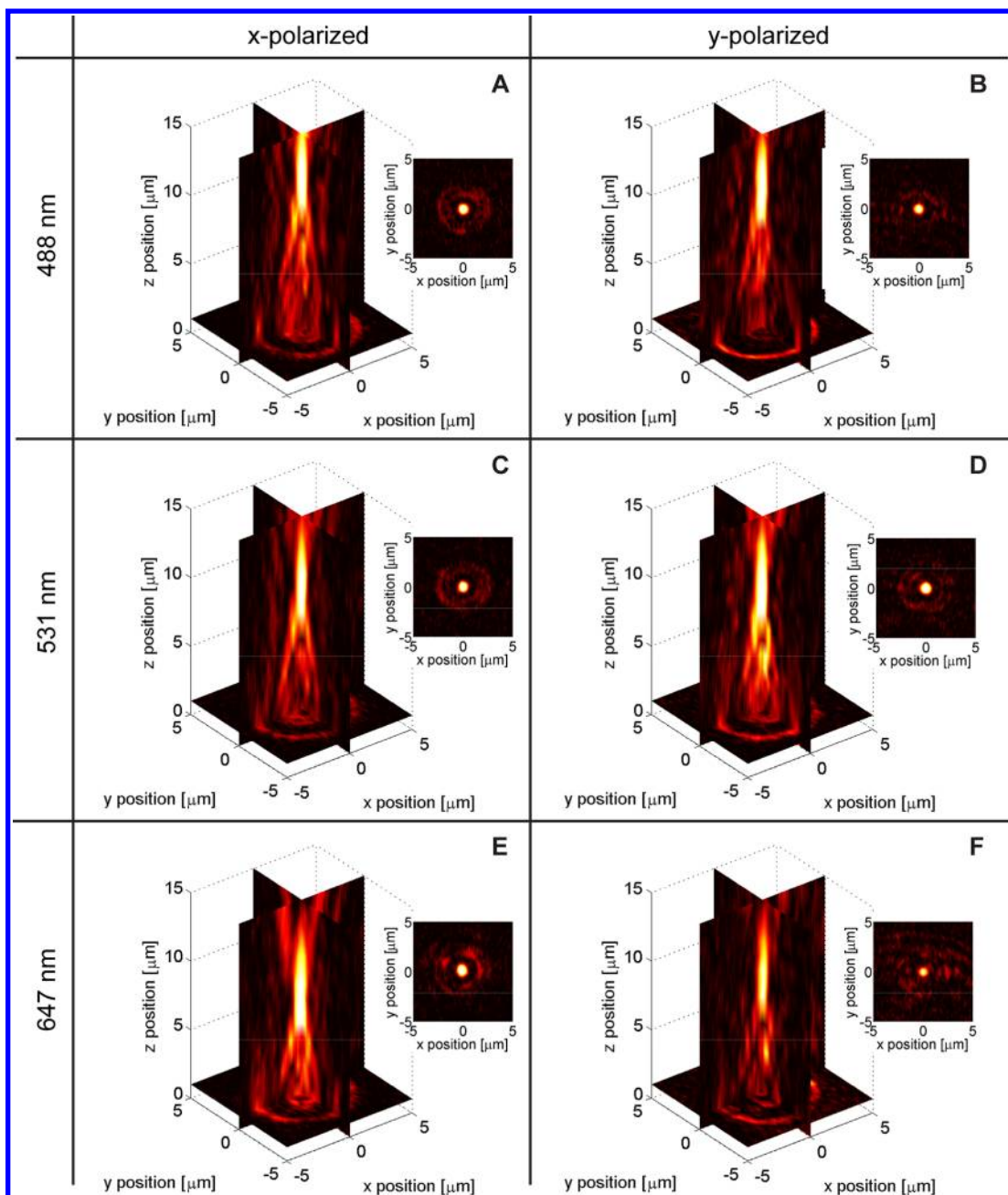


Figure 5. Pseudocolor cross-section intensity maps measured experimentally at various heights above the sample surface for x-polarized (A, C, E) and y-polarized incident light (B, D, F) at 488 nm (A, B), 531 nm (C, D), and 647 nm (E, F). The x - y planes are at $z = 1 \mu\text{m}$, the y - z planes are at $x = 0$, and the z - x planes are at $y = 0$. The insets show the beam x - y cross sections at the focus for each wavelength (for A and B, $z = 12 \mu\text{m}$; for C and D, $z = 10 \mu\text{m}$; for E and F, $z = 8 \mu\text{m}$).

properties of binary Fresnel zone plates, but this design is built on very different operational principles. In contrast to photon sieves, which deal with multimode intensities diffracted by holes with wavelength-scale diameters, our device is built on wavefront engineering using single-mode phase shifts obtained from subwavelength-diameter holes.

A circular hole milled into a metallic film can be considered as a finite-length circular waveguide with a metal cladding. Note that the electromagnetic fields in the optical range penetrate into metal cladding because the magnitude of the metal permittivity is not that large (around 1 or 2). Therefore, the propagating hybrid modes are excited in the structure, and below the surface plasmon frequency, the only propagating

mode in a subwavelength hole is the HE_{11} mode.^{32,33} Hence in this structure a single-mode regime is achieved.

Similar to the dependence of the output phase on the width for metal slits, we show in this work that the phase of the light coming through a hole is a function of the hole radius. We used a three-dimensional, spatial analysis method³⁴ to simulate a hole milled in a 380-nm-thick gold film and illuminated with a 531 nm, linearly polarized plane wave from the glass substrate side. To increase the cutoff frequency, we assumed the hole is filled with poly(methyl methacrylate) (PMMA) whose refractive index is 1.5. This also matches the real experimental situation in which there is a 200 nm PMMA layer on top of the film (see experimental description below). The relative phases

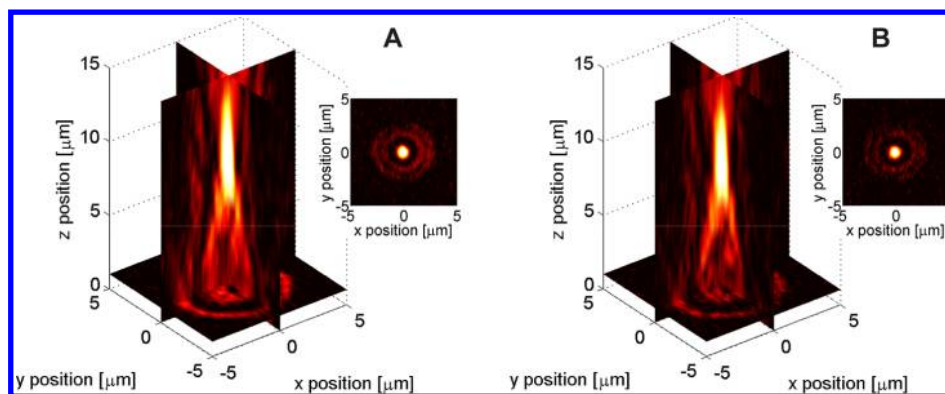


Figure 6. Experimentally measured transmission through the sample for left circularly polarized (A) and right circularly polarized incident light (B) at a wavelength of 531 nm. In panels A and B, the x - y planes are at $z = 1 \mu\text{m}$, the y - z planes are at $x = 0$, and the z - x planes are at $y = 0$. The insets show the beam x - y cross sections at $z = 10 \mu\text{m}$.

of the output are evaluated in the far field. The results of these calculations, shown in Figure 2, clearly indicate that the mode index and phase increase as the hole radius decreases, and the field becomes more confined. This dependence is similar to plasmonic-mode propagation through a metallic slit.¹⁹ In addition, the same design was numerically examined for circularly polarized incident light, and phase control is also predicted in this case (see Figure 2).

Once the phase-radius dependence is obtained, a focusing holey-metal lens can be designed. To design such a device, we developed a simple analytical model based on the 3D Green's function; this is similar to the 2D Green's function that has been used to design our previous nanoslit lenses.²¹ Using the reciprocity principle, we located a dipole point source emitting light with a free-space wavelength λ_0 at the desired focal point $F(0, 0, f)$ of the system, where f is the focal length. In 3D space and in the far field, the electromagnetic field emitted from a point source is proportional to the Green's function given by $G(r) = e^{ikr}r^{-1}$, where $r = (x^2 + y^2 + (z - f)^2)^{1/2}$ and $k = 2\pi\lambda_0^{-1}$. The phase at the sample surface $\phi(x, y, 0)$ relative to the origin $O(0, 0, 0)$ is retrieved by taking the argument of the Green's function. We then model the array of holes in the metallic film using a discrete dipole approximation in which we assign a phase of $-\phi(x, y, 0)$ to each dipolar source and locate the sources at discrete locations on the sample's metallic surface where the holes would exist. We then calculate the resultant total intensity from the array of phase-shifted dipoles. The intensity map of the device for $f = 10 \mu\text{m}$ and $\lambda_0 = 531 \text{ nm}$ is plotted in Figure 3. The locations of the dipolar sources correspond to the center positions of the holes in Figure 3. As we show later, the intensity map calculated from this computationally inexpensive analytical model captures the major features of the experimentally measured results.

In experiment, we fabricated the holey metal lens as well as the slit-ring lens schematically shown in Figure 1B. We created our experimental samples by first depositing a 380-nm-thick gold film on a glass substrate. The holes were then milled through the gold film by a focused ion beam (FIB, FEI nova200) system as shown in the SEM image (see Figure 4). The detailed structure of the sample is summarized in Table 1. After the FIB fabrication, a 200 nm PMMA film was spin-coated on the sample, followed by baking at 90 s at 180 °C. The PMMA filled the holes and remained as a 200-nm-thick uniform film on the gold surface. At the positions of the holes, we observed only slight ($\sim 20 \text{ nm}$) pits in the PMMA layer.

Filling the holes with polymer increases the refractive index within the holes and hence decreases the cutoff radius at a particular frequency.²¹ The transmission intensities of the sample at 488, 531, and 647 nm in two orthogonal linear polarizations were recorded using a microscope and a CCD camera. At 531 nm, the transmission intensities were also recorded under circularly polarized incidence. The sample was illuminated from the substrate side at normal incidence. The resolution of the microscope stage in z axis was $\pm 250 \text{ nm}$, and the depth of field of the microscope setup is about 500 nm. More details on the used setup can be found in our previous work.²¹ Note that the slit-ring sample shown in Figure 1C has identical concentric radii as the sample shown in Figure 4, and each ring width given by the corresponding hole diameter of the sample as shown in Table 1. The fabrication of the slit-ring sample and its optical measurements were done in the same way as described above.

In Figure 5 we show a summary of the transmission measurements from the sample illuminated by x -polarized light and y -polarized light for the three different wavelengths (488, 531, and 647 nm). Identical focal lengths of $10 \mu\text{m}$ were obtained for 531 nm illumination at both polarizations. We therefore conclude that the lens focuses the incident light as expected in the original design. Compared to Figure 3, the experimental profiles have higher background than the simulated profiles. The discrepancies between the experimental results and the simulations could be due to imperfection of the hole shapes as well as possible damage in the metal hole edges by gallium ions during the FIB fabrication.³⁵ Nevertheless, we can utilize the analytical model for rapid prototyping, with a possible further optimization of devices through full-wave finite element modeling (similar to ref 21). The insets in Figure 5C and D show the pseudocolor x - y maps of the intensity at the focus. The focus profiles do not depend on the incident polarization, and the focus spots are circular, which is different from the focus spot shown in Figure 1E for the slit-ring design. The focal lengths for both polarizations at 488 and 647 nm are 8 and $12 \mu\text{m}$, respectively. Hence by changing the incident wavelength, we can shift the focal distance of the lens. Even at those wavelengths, the focus profiles show little dependence to the incident polarizations.

Figure 6A and B shows the measured results at 531 nm for left circularly polarized and right circularly polarized incident light, respectively. As expected from Figure 2, the focal lengths as well as the focusing profiles for left and right circular

polarizations are quite similar to the results shown in Figure 5C and D.

In summary, we have experimentally demonstrated polarization-independent performance of holey-metal lenses. First, we showed that, by changing the radii of subwavelength holes in a metallic film, which act as single-mode waveguide elements, we can control the phase of light transmitted through the holes. Then, by placing multiple holes with different radii to form a concave phase front, we experimentally demonstrated the focusing property of a device with multiple holes in a gold film. Finally, we demonstrated that the focal distance of the lens can be controlled by changing the incident wavelength. Our design is simple and planar, and thus it allows for high-throughput fabrication methods such as nanoimprint lithography³⁶ or laser dynamic forming.³⁷ The planar and compact design of the lens is beneficial for obtaining short focal distances on the order of one micrometer for on-chip devices and fiber-coupled probes.¹

AUTHOR INFORMATION

Corresponding Author

*E-mail: kildishev@purdue.edu.

Notes

The authors declare no competing financial interest.

ACKNOWLEDGMENTS

Authors would like to thank V. P. Drachev for instrumental discussions and suggestions regarding optical measurements. A.V.K. is partially supported by the AFRL Materials and Manufacturing Directorate Applied Metamaterials Program. S.I. is supported by the Japan Society for the Promotion of Science (JSPS) Postdoctoral Fellowships for Research Abroad. V.M.S. is supported by the ONR MURI grant N00014-010942 "Large-Area, 3D Optical Metamaterials with Tunability and Low Loss" and NSF DMR grant 1120923. Author contributions are as follows: S.I. designed the sample outline, fabricated the sample, and performed optical measurements. A.V.K. proposed the design concept and the modeling principles, validated the numerical simulations, and supervised the project. All of the authors were involved in discussing the project and writing the manuscript.

REFERENCES

- (1) Prasciolu, M.; Cojoc, D.; Cabrini, S.; Businaro, L.; Candeloro, P.; Tormen, M.; Kumar, R.; Liberale, C.; Degiorgio, V.; Gerardino, A. *Microelectron. Eng.* **2003**, *67*, 169–174.
- (2) Liu, Y.; Jiong, H. *J. Micro/Nanolith. MEMS MOEMS* **2010**, *9*, 033004.
- (3) Liu, Y.; Liu, H.; He, L.; Zhou, H.; Sui, C. *Opt. Laser Technol.* **2010**, *42* (8), 1286–1293.
- (4) Pendry, J. B. *Phys. Rev. Lett.* **2000**, *85* (18), 3966–3969.
- (5) Fang, N.; Lee, H.; Sun, C.; Zhang, X. *Science* **2005**, *308* (5721), 534–537.
- (6) Melville, D. O. S.; Blaikie, R. J. *Opt. Express* **2005**, *13* (6), 2127–2134.
- (7) Jacob, Z.; Alekseyev, L. V.; Narimanov, E. *Opt. Express* **2006**, *14* (18), 8247–8256.
- (8) Salandrino, A.; Engheta, N. *Phys. Rev. B* **2006**, *74* (7), 075103.
- (9) Liu, Z.; Lee, H.; Xiong, Y.; Sun, C.; Zhang, X. *Science* **2007**, *315* (5819), 1686.
- (10) Smolyaninov, I. I.; Hung, Y. J.; Davis, C. C. *Science* **2007**, *315* (5819), 1699.
- (11) Liu, Z.; Steele, J. M.; Srituravanich, W.; Pikus, Y.; Sun, C.; Zhang, X. *Nano Lett.* **2005**, *5* (9), 1726–1729.
- (12) Yin, L.; Vlasko-Vlasov, V. K.; Pearson, J.; Hiller, J. M.; Hua, J.; Welp, U.; Brown, D. E.; Kimball, C. W. *Nano Lett.* **2005**, *5* (7), 1399–1402.
- (13) Huang, F. M.; Zheludev, N.; Chen, Y.; de Abajo, F. J. G. *Appl. Phys. Lett.* **2007**, *90*, 091119.
- (14) Huang, F. M.; Kao, T. S.; Fedotov, V. A.; Chen, Y.; Zheludev, N. I. *Nano Lett.* **2008**, *8* (8), 2469–2472.
- (15) Rogers, E. T. F.; Lindberg, J.; Roy, T.; Savo, S.; Chad, J. E.; Dennis, M. R.; Zheludev, N. I. *Nat. Mater.* **2012**, *11* (5), 432–435.
- (16) Fu, Y.; Zhou, X. *Plasmonics* **2010**, 1–24.
- (17) Aieta, F.; Genevet, P.; Kats, M. A.; Yu, N.; Blanchard, R.; Gaburro, Z.; Capasso, F. *Nano Lett.* **2012**, *12*, 1702–1706.
- (18) Sun, Z.; Kim, H. K. *Appl. Phys. Lett.* **2004**, *85*, 642–644.
- (19) Shi, H.; Wang, C.; Du, C.; Luo, X.; Dong, X.; Gao, H. *Opt. Express* **2005**, *13* (18), 6815–6820.
- (20) Verslegers, L.; Catrysse, P. B.; Yu, Z.; White, J. S.; Barnard, E. S.; Brongersma, M. L.; Fan, S. *Nano Lett.* **2009**, *9* (1), 235–238.
- (21) Ishii, S.; Kildishev, A. V.; Shalaev, V. M.; Chen, K. P.; Drachev, V. P. *Opt. Lett.* **2011**, *36* (4), 451–453.
- (22) Ishii, S.; Kildishev, A. V.; Shalaev, V. M.; Drachev, V. P. *Laser Phys. Lett.* **2011**, *8*, 828–832.
- (23) Fu, Y.; Zhou, W.; Lim, L.; Du, C.; Luo, X. *Appl. Phys. Lett.* **2007**, *91* (6), 061124–061124–3.
- (24) Fu, Y.; Zhou, W.; Lim, L. E. N. *J. Opt. Soc. Am. A* **2008**, *25* (1), 238–249.
- (25) Shi, Z.; Fu, Y.; Zhou, X.; Zhu, S. *Plasmonics* **2010**, *5* (2), 175–182.
- (26) Gao, H.; Hyun, J. K.; Lee, M. H.; Yang, J.-C.; Lauhon, L. J.; Odom, T. W. *Nano Lett.* **2010**, *10* (10), 4111–4116.
- (27) Kipp, L.; Skibowski, M.; Johnson, R.; Berndt, R.; Adelung, R.; Harm, S.; Seemann, R. *Nature* **2001**, *414* (6860), 184–188.
- (28) Cao, Q.; Jahns, J. *J. Opt. Soc. Am. A* **2002**, *19* (12), 2387–2393.
- (29) Andersen, G. *Opt. Lett.* **2005**, *30* (22), 2976–2978.
- (30) Menon, R.; Gil, D.; Barbastathis, G.; Smith, H. I. *J. Opt. Soc. Am. A* **2005**, *22* (2), 342–345.
- (31) Cao, Q.; Jahns, J. *J. Opt. Soc. Am. A* **2006**, *23* (1), 179–186.
- (32) Pfeiffer, C. A.; Economou, E. N.; Ngai, K. L. *Phys. Rev. B* **1974**, *10* (8), 3038–3051.
- (33) Shin, H.; Catrysse, P. B.; Fan, S. *Phys. Rev. B* **2005**, *72* (8), 085436.
- (34) Ni, X.; Liu, Z.; Boltasseva, A.; Kildishev, A. V. *Appl. Phys. A: Mater. Sci. Process.* **2010**, *100* (2), 365–374.
- (35) Leen, J. B.; Hansen, P.; Cheng, Y. T.; Hesselink, L. *Opt. Lett.* **2008**, *33* (23), 2827–2829.
- (36) Chou, S. Y.; Krauss, P. R.; Renstrom, P. J. *Science* **1996**, *272* (5258), 85–87.
- (37) Gao, H.; Ye, C.; Cheng, G. J. *J. Manuf. Sci. Eng.* **2009**, *131*, 5.